Experimental Observation of a Generalized Thouless Pump with a Single Spin

Wenchao Ma,[1,2] Longwen Zhou,[3] Qi Zhang,[1,2] Min Li,[1,2] Chunyang Cheng,[1,2] Jianpei Geng,[1,*] Xing Rong,[1,2,4] Fazhan Shi,[1,2,4,†] Jiangbin Gong,[3,‡] and Jiangfeng Du[1,2,4,§]

[1]*CAS Key Laboratory of Microscale Magnetic Resonance and Department of Modern Physics, University of Science and Technology of China, Hefei 230026, China*

[2]*Synergetic Innovation Center of Quantum Information and Quantum Physics, University of Science and Technology of China, Hefei 230026, China*

[3]*Department of Physics, National University of Singapore, Singapore 117543, Singapore*

[4]*Hefei National Laboratory for Physical Sciences at the Microscale, University of Science and Technology of China, Hefei 230026, China*

(Received 7 August 2017; revised manuscript received 17 January 2018; published 19 March 2018)

Adiabatic cyclic modulation of a one-dimensional periodic potential will result in quantized charge transport, which is termed the Thouless pump. In contrast to the original Thouless pump restricted by the topology of the energy band, here we experimentally observe a generalized Thouless pump that can be extensively and continuously controlled. The extraordinary features of the new pump originate from interband coherence in nonequilibrium initial states, and this fact indicates that a quantum superposition of different eigenstates individually undergoing quantum adiabatic following can also be an important ingredient unavailable in classical physics. The quantum simulation of this generalized Thouless pump in a two-band insulator is achieved by applying delicate control fields to a single spin in diamond. The experimental results demonstrate all principal characteristics of the generalized Thouless pump. Because the pumping in our system is most pronounced around a band-touching point, this work also suggests an alternative means to detect quantum or topological phase transitions.

DOI: 10.1103/PhysRevLett.120.120501

In 1983, Thouless discovered that the charge transport across a one-dimensional lattice over an adiabatic cyclic variation of the lattice potential is quantized, equaling to the first Chern number defined over a Brillouin zone formed by quasimomentum and time [1]. This phenomenon, known as the Thouless pump, shares the same topological origin as the quantization of Hall conductivity [2–4] and may thus be regarded as a dynamical version of the integer quantum Hall effect [5]. In the ensuing years, the Thouless pump was investigated extensively [4]. Up to now, several single-particle pumping experiments have been implemented in nanoscale devices [6–9]. Most recently, the Thouless pump was observed in cold atom systems [10,11]. On the application side, the Thouless pump has the potential for realizing novel current standards [12,13], characterizing many-body systems [14–18], and exploring higher dimensional physics [19].

In Thouless' original proposal and almost all the follow-up studies, the initial-state quantum coherence between different energy bands, namely, the interband coherence in the initial states, is not taken into account. As a fundamental feature of quantum systems [20,21], quantum coherence is at the root of a number of fascinating phenomena in chemical physics [22–24], quantum optics [25–29], quantum information [30], quantum metrology [31–33], solid-state physics [34,35], thermodynamics [36–40], magnetic resonance [41–43], and even biology [44–46]. Therefore, a question naturally arises as to how the pump will behave if the interband coherence resides in the initial state. A theoretical analysis of this issue is outlined in Fig. 1, where Q_a and Q_b represent pumping contributed by

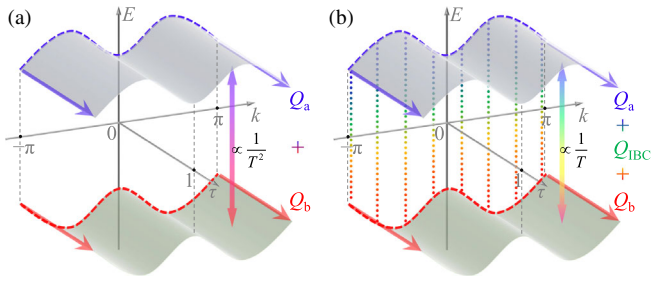

FIG. 1. Illustration about how interband coherence in the initial state leads to the generalized Thouless pump of duration T. Band dispersion relations are plotted via energy and quasimomentum variables E vs k, and τ represents the time scaled by T. (a) With an initial state being an incoherent mixture of states from different bands, the nonadiabatic correction to the band populations is of the order of $1/T^2$. The resultant pumping $Q_a + Q_b$ is a weighted sum of the contribution from each band. (b) With an initial state having interband coherence, the pumping operation induces a population correction of the order of $1/T$, whose effect accumulated over T yields a pumping term Q_{IBC} that is T independent and continuously tunable.

individual bands, and Q_{IBC} is fueled by interband coherence [47,48]. In contrast to the conventional Thouless pump where the pumping components Q_a and Q_b are determined by the Berry curvature of each filled band, the generalized Thouless pump is featured by the component Q_{IBC} that can be continuously and extensively controlled. The main aspects of Q_{IBC} are experimentally investigated in this work.

Consider a one-dimensional two-band insulator subject to time-dependent modulations. Its Hamiltonian in the quasimomentum space is

$$H(k,\tau)=\frac{\omega\sin k}{2}[\cos\phi(\tau)\sigma_x+\sin\phi(\tau)\sigma_y]+\frac{\delta_1\cos k+\delta_2}{2}\sigma_z. \tag{1}$$

Throughout, $\tau=t/T$ is the scaled time with t being the real time and T the duration of one pumping cycle, $k\in(-\pi,\pi]$ is the quasimomentum, $\sigma_{x,y,z}$ are the Pauli matrices, and $\hbar$ is set to 1. The instantaneous spectrum of $H(k,\tau)$ is gapless at $k=0\,(k=\pi)$ when and only when $\delta_1=-\delta_2$ $(\delta_1=\delta_2)$. One pumping cycle can be realized by slowly varying ϕ from 0 to 2π. In a lattice representation, the parameters δ_1 and δ_2 represent the respective bias in the nearest-neighbor hopping strength and energy between two internal states.

For a general initial state with equal populations on quasimomenta k and $-k$ on each band, the pumped amount of charge Q over N adiabatic cycles can be found from the first-order adiabatic perturbation theory (APT) [47–50], where $Q=N(Q_{\mathrm{TP}}+Q_{\mathrm{IBC}})+Q_{\mathrm{NG}}$, with

$$Q_{\mathrm{TP}}=\frac{1}{2\pi}\int_{-\pi}^{\pi}dk\sum_n\rho_{nn}|_{\tau=0}\int_0^1 d\tau\Omega_{\tau k}^{(n)}, \tag{2}$$

$$Q_{\mathrm{IBC}}=\frac{1}{2\pi}\int_{-\pi}^{\pi}dk\sum_{m,n(m<n)}\frac{2\mathrm{Im}(\rho_{mn}\langle n|\partial_\tau|m\rangle)}{E_m-E_n}\Big|_{\tau=0}\times\int_0^1 d\tau(v_{mm}-v_{nn}), \tag{3}$$

and Q_{NG} being a nongeneric term that does not build up with the number of pumping cycles (hence not of interest here) [51]. That is, only Q_{TP} and Q_{IBC} represent contributions from pumping over each adiabatic cycle. In above m and n are band indices, $|m(k,\tau)\rangle$ represent an instantaneous eigenstate of $H(k,\tau)$ with the eigenvalue $E_m(k,\tau)$, $\rho_{mn}(k,\tau)$ and $v_{nm}(k,\tau)$ refer to matrix elements of the density operator and the velocity operator $v(k,\tau)\equiv\partial_k H(k,\tau)$ in representation of $|m(k,\tau)\rangle$, and $\Omega_{\tau k}^{(n)}$ is the Berry curvature of the nth instantaneous energy band of $H(k,\tau)$. The component Q_{TP} $(=Q_a+Q_b$ in the case of Fig. 1), representing a weighted integral of the Berry curvature, was found previously by Thouless [1]. The component Q_{IBC}, namely, the charge pumping induced by interband coherence in the initial state, is responsible for the generalized Thouless pump and will be our focus here. Analogous to the conventional Thouless pumping, Q_{IBC} arises from an accumulation of small nonadiabatic effects over one pumping cycle. As sketched in Fig. 1, the initial-state interband coherence plays a crucial role in generating the underlying nonadiabatic effects. The term Q_{IBC} is found to be nontopological and can change continuously. As indicated by Eq. (2), Q_{IBC} depends on $\langle n|\partial_\tau|m\rangle|_{\tau=0}$ and the band gap. For a pumping parameter $\phi(\tau)$ as in our two-band model depicted in Eq. (1), one has $\langle n|\partial_\tau|m\rangle|_{\tau=0}\sim[d\phi(\tau)/d\tau]|_{\tau=0}$, which can be controlled by the switching-on rate of a pumping protocol. The band gap in our model can be altered via tuning δ_1/δ_2 and Q_{IBC} can even diverge logarithmically as the band gap is tuned to approach zero [51].

The generalized Thouless pump can be experimentally realized on a qubit system because the insulator's Hamiltonian in Eq. (1) is also the Hamiltonian of a qubit in a rotating field parametrized by k and ϕ. That is, by mapping the two-band insulator's Hamiltonian to that for a qubit in a rotating field, we can experimentally demonstrate the generalized Thouless pump using a single spin [52]. To highlight the contribution from Q_{IBC}, in our experiment the initial state is properly designed such that $Q_{\mathrm{TP}}=Q_{\mathrm{NG}}=0$; i.e., the traditional Thouless pumping and the nongeneric term Q_{NG} have no contribution. To demonstrate the sensitivity of Q_{IBC} to the switching-on rate of the pumping protocol, namely, $[d\phi(\tau)/d\tau]|_{\tau=0}$, we consider a linear ramp $\phi(\tau)=2\pi\tau$ and a quadratic ramp $\phi(\tau)=2\pi\tau^2$. One directly sees that the latter choice with zero switching-on rate will make $Q_{\mathrm{IBC}}=0$ within the first-order APT. To demonstrate the dependence of Q_{IBC} on the band gap, we implement the Hamiltonian in Eq. (1) with a varying band gap.

A negatively charged nitrogen-vacancy (NV) center in diamond is used in the experiment. As shown in Fig. 2(a), the NV center is composed of one substitutional nitrogen atom and an adjacent vacancy [53–56]. In our experiment, an external static magnetic field around 510 G is parallel to the NV symmetry axis. Such magnetic field enables both the NV electron spin and the host ^{14}N nuclear spin to be polarized by optical excitation [57,58]. As illustrated in Fig. 2(b), microwaves generated by an arbitrary waveform generator drives the transition between the electronic levels $|m_s=0\rangle$ and $|m_s=-1\rangle$ which compose a qubit, and the level $|m_s=1\rangle$ remains idle due to large detuning [59]. The Hamiltonian of the qubit in the laboratory frame is $H^{\mathrm{lab}}=\omega_0\sigma_z/2+f(t)\sigma_x$, where the term $f(t)\sigma_x$ delineates the effect of the microwave field. The expectation value of the observable σ_z can be read out via fluorescence detection during optical excitation. All the optical procedures are performed on a home-built confocal microscope, and a solid immersion lens is etched on the diamond above the NV center to enhance the fluorescence collection [60,61].

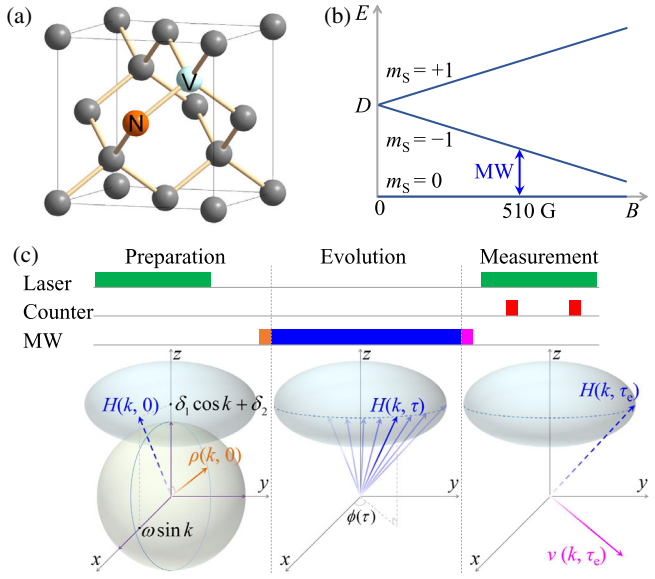

FIG. 2. Experimental system and method. (a) NV center in diamond. (b) Electronic ground state of a negatively charged NV center. The energy splitting depends on the magnetic field which is parallel to the NV axis in this experiment [59]. The two levels $|m_s = 0\rangle$ and $|m_s = -1\rangle$ are encoded as a qubit which is manipulated by microwaves (MW). (c) Pulse sequence for qubit control and measurement. The ellipsoid surface represents the parameter space and the sphere represents the Bloch sphere.

In our work, the experiment for different k is performed separately in different runs of experiment. The pulse sequence for each k is sketched in Fig. 2(c). At first, the qubit is polarized to the state $\rho_0 = (\mathbb{1} + \sigma_z)/2$ by a laser pulse [see the green bar in the preparation section in Fig. 2(c)], and then the initial state $\rho(k, 0)$ needs to be prepared. To optimize Q_{IBC} in the experiment, the initial density matrix $\rho(k, 0)$ at individual values of k is designed such that its associated Bloch vector is perpendicular to the direction of the field that yields $H(k, 0)$. This choice is again illustrated in Fig. 2(c). Specifically, $\rho(k, 0)$ is chosen as $[\mathbb{1} + \boldsymbol{n}(k) \cdot \boldsymbol{\sigma}]/2$ with the unit vector $\boldsymbol{n}(k)$ along the direction $(-\delta_1 \cos k - \delta_2, 0, \omega \sin k)$ except that $\boldsymbol{n} = (0, 0, 1)$ at a band touching point. This choice also makes Q_{TP} and Q_{NG} vanish [51]. To prepare such an initial state, we apply a resonance microwave pulse with the temporal dependence $f(t) = \omega_1 \cos(\omega_0 t + \varphi_{\mathrm{ini}})$, where the time t starts from zero, ω_1 is the Rabi frequency, and the initial phase φ_{ini} is set as $-\pi/2\,(\pi/2)$ if $\delta_1 \cos\theta + \delta_2 \geq 0\,(< 0)$. The duration of the pulse is $t_{\mathrm{ini}} = \alpha/\omega_1$, where α is the inclination angle of $\boldsymbol{n}(k)$. The orange bar in the preparation section in Fig. 2(c) represents this pulse.

Upon initial-state preparation, the qubit is left to evolve under $H(k, \tau)$, namely, in the presence of a field whose transverse and longitudinal magnitudes are given by $\omega \sin k$ and $\delta_1 \cos k + \delta_2$, respectively. The field is then rotated around the z axis according to $\phi(\tau)$, with $\phi(\tau)$ understood as the azimuthal angle. This rotating field is implemented by applying a microwave pulse with $f(t) = \omega \sin k \cos[(\omega_0 - \delta_1 \cos k - \delta_2)t + \phi(\tau) + \varphi_{\mathrm{I}}]$, where t starts from zero and the initial phase $\varphi_{\mathrm{I}} = \omega_0 t_{\mathrm{ini}}$ is used to match the phase of the first pulse. In Fig. 2(c) this pulse is depicted by the blue bar in the evolution section. In a frame with the initial azimuthal angle φ_{I} and rotating around the z axis with the angular frequency $\omega_0 - \delta_1 \cos k - \delta_2$ relative to the laboratory frame, the bare Hamiltonian H^{lab} is transformed, via the rotation transformation operator $e^{-i[(\omega_0 - \delta_1 \cos k - \delta_2)t + \varphi_{\mathrm{I}}]\sigma_z/2}$, to our target Hamiltonian $H(k, \tau)$ under the rotating wave approximation. The parameters adopted in our experiment are $\omega = 2\pi \times 20$ MHz, $\delta_1 = 2\pi \times 10$ MHz, and δ_2 between 0 to $2\pi \times 20$ MHz.

The evolution governed by $H(k, \tau)$ lasts for some duration $t_e \in [0, T]$ (with the corresponding scaled time $\tau_e \in [0, 1]$), and then the velocity $v(k, \tau_e)$ needs to be measured. As shown in Fig. 2(c), the measurement procedure begins with a microwave pulse (the magenta bar). This pulse is described by $f(t) = \omega_1 \cos(\omega_0 t + \varphi_{\mathrm{I}} + \varphi_{\mathrm{II}} + \varphi_{\mathrm{fin}})$, with t starting from zero, $\varphi_{\mathrm{II}} = (\omega_0 - \delta_1 \cos k - \delta_2)t_e + \phi(\tau_e)$, and $\varphi_{\mathrm{fin}} = -\pi/2\,(\pi/2)$ when $\cos k \geq 0\,(< 0)$. The duration of the pulse is $t_{\mathrm{fin}} = \beta/\omega_1$, where β is the inclination angle of the direction of v. This resonant microwave pulse, which steers the direction of $v(k, \tau_e)$ to the $+z$ direction, is followed by a laser pulse [the right green bar in Fig. 2(c)] together with fluorescence detection. The fluorescence is collected via two counting windows represented by the two red bars in Fig. 2(c). The former window records the signal while the latter records the reference [51]. The fluorescence collection amounts to the measurement of σ_z, and the effect combined with the microwave pulse is equivalent to the observation of $v(k, \tau_e)/\|v\|$, where $\|v\|$ is the spectral norm of v.

The above sequence is performed for a series of $\tau_e \in [0, 1]$, and is iterated at least a hundred thousand times to obtain the expectation value. One can then get $\langle v(k, \tau)\rangle/\|v\|$ as a function of τ. Numerical integration over τ based on these experimental data, multiplied by $\|v\|$, yields the experimental value of $q(k) = T\int_0^1 \langle v(k, \tau)\rangle d\tau$, the pumped charge contributed from a certain k. This procedure is repeated for different values of $k \in [0, \pi]$. Some experimental data with $T = 1$ μs and $\phi(\tau) = 2\pi\tau$ are instantiated in Fig. 3. The pattern of the normalized velocity $\langle v(k, \tau)\rangle/\|v\|$ depends strongly on δ_2/δ_1, and so does the shape of $q(k)$. In particular, there is a significant charge transport for $\delta_2/\delta_1 \approx 1$ and $k \approx \pi$, i.e., near the band touching point.

Because of the symmetry considerations, it suffices to let our measurements cover half of the first Brillouin zone to extract the pumped charge $Q = \int_{-\pi}^{\pi} q(k)dk/(2\pi) = \int_0^{\pi} q(k)dk/\pi$ [51]. As illustrated by the orange curve and data points in Fig. 4(a), the pumped charge Q first rises and then declines as the parameter δ_2/δ_1 sweeps from 0 to 2. The parameter δ_2/δ_1 also determines the band gap as

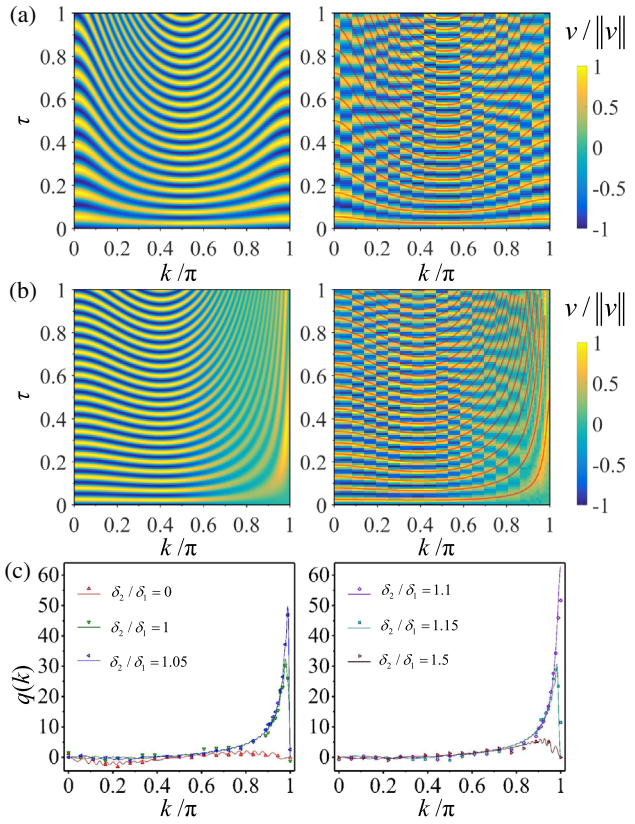

FIG. 3. Normalized velocity expectation values and pumped charge per each k. (a), (b) Normalized value $\langle v\rangle/\|v\|$ vs k and τ for $\delta_2/\delta_1 = 0$ and 1, respectively. Experimental data (calculations based on the Schrödinger equation) are on the right (left). The red curves in the experimental figures are guides to the eye to clarify the patterns in the color map. These guidelines are the crest lines in the patterns of the calculated $\langle v\rangle/\|v\|$. (c) Pumped charge $q(k)$ per each synthetic quasimomentum k for several values of δ_2/δ_1. Symbols (curves) represent the experimental data (the calculation).

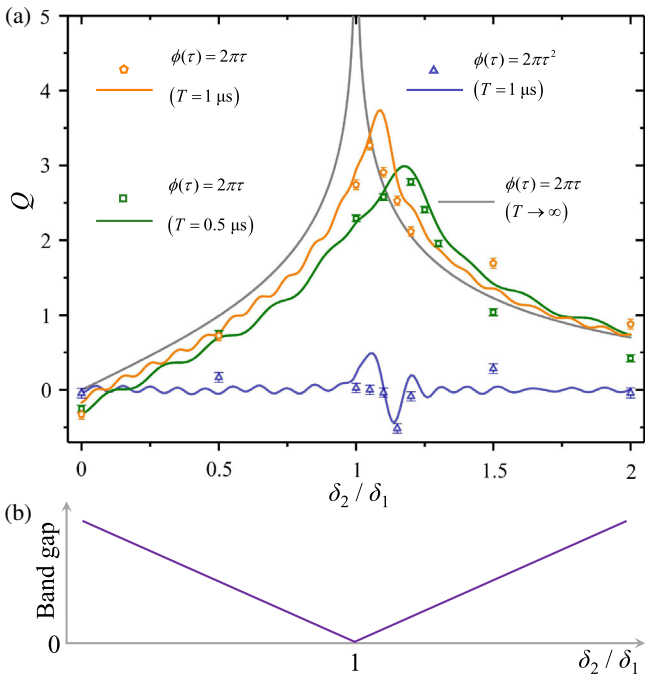

FIG. 4. Transported charge Q and band gap vs δ_2/δ_1. (a) The symbols and curves represent experimental data and theoretical results, respectively. The orange symbols and curve are for the linear ramp $\phi(\tau) = 2\pi\tau$ with $T = 1\ \mu$s. The green symbols and curve are for $\phi(\tau) = 2\pi\tau$ with $T = 0.5\ \mu$s. The grey theoretical curve corresponds to $\phi(\tau) = 2\pi\tau$ with $T \to \infty$. The blue symbols and curve correspond to the parabolic ramp $\phi(\tau) = 2\pi\tau^2$ with $T = 1\ \mu$s. Error bars represent ± 1 s.d. (b) In the two-band model, the band gap is $|\delta_2 - \delta_1|$.

sketched in Fig. 4(b). Though the ramp time $T = 1\ \mu$s is still not in the true adiabatic limit $T \to \infty$, the pumped charge Q for $T = 1\ \mu$s as a function of δ_2/δ_1 bears strong resemblance with the theoretical curve for $T \to \infty$ obtained using the first-order APT, with their differences well accounted for. In particular, the theoretical logarithmic divergence of Q as $\delta_2/\delta_1 \to 1$ [see the gray curve in Fig. 4(a)] implicitly requires $T \to \infty$ as the condition to apply the first-order APT. The actual observed pumping for a finite $T = 1\ \mu$s is thus not expected to shoot to infinity. In addition, the peak of Q is not precisely at $\delta_2/\delta_1 = 1$, but has a rightward shift. In this linear ramp case, a nonperturbative theory can be developed [51]. The theoretical shift of the peak of Q as a function of δ_2/δ_1 is found to be $2\pi/(\delta_1 T)$, in good agreement with our observation. This clearly indicates that the observed peak shift is merely a finite-T effect. For a shorter ramp time $T = 0.5\ \mu$s as depicted by the green curve and data points in Fig. 4(a), the pumping peak slightly goes lower again and shifts further away from the exact phase transition point $\delta_2/\delta_1 = 1$. Overall, the two pumping curves with $T = 1\ \mu$s and $T = 0.5\ \mu$s have a remarkable overlap with each other, thus supporting that to the zeroth order of $1/T$, the outcome of the generalized Thouless pump is independent of T. We next investigate another pumping protocol $\phi(\tau) = 2\pi\tau^2$ with $T = 1\ \mu$s. The initial switching-on rate of this pumping protocol now vanishes. In this case, we observe negligible pumping, as evidenced by the blue curve and data points in Fig. 4(a). The results for the two different protocols confirm that the generalized Thouless pump can be extensively tuned by varying the switching-on rate of a pumping protocol. Finally, one may note the differences between experimental results and the simulation results [orange, green, and blue solid curves in Fig. 4(a)] based solely on time-dependent Schrödinger equations. The experimental errors are mainly due to the imperfection of the microwave pulses. Nevertheless, in the presence of the experimental errors, our experimental results have demonstrated all principal features of the generalized Thouless pump.

In conclusion, by incorporating interband coherence into the initial state as a powerful quantum resource, we are able to go beyond the traditional Thouless pump. Using a single spin in diamond, we have experimentally demonstrated a novel type of quantum adiabatic pump, which is extensively

and continuously tunable by varying the switching-on rate of a pumping protocol. The tunability of our generalized Thouless pump is reminiscent of the famous Archimedes screw, where water is pumped via rotating a screw-shaped blade in a cylinder and the amount of pumped water can also be changed continuously [62–64]. Furthermore, because the coherence-based pumping in our system is most pronounced around a band-touching point, it may provide an alternative means for the detection of band touching and hence quantum or topological phase transition points. Our work thus enriches the physics of adiabatic pump and coherence-based quantum control.

The authors at University of Science and Technology of China are supported by the National Natural Science Foundation of China (Grants No. 81788101, No. 11227901, No. 31470835, No. 91636217, and No. 11722544), the CAS (Grants No. GJJSTD20170001, No. QYZDY-SSW-SLH004, No. QYZDB-SSW-SLH005, and No. YIPA2015370), the 973 Program (Grants No. 2013CB921800, No. 2016YFA0502400, and No. 2016YFB0501603), the CEBioM, and the Fundamental Research Funds for the Central Universities (WK2340000064). The authors at National University of Singapore are supported by the Singapore NRF Grant No. NRF-NRFI2017-04 (WBS No. R-144-000-378-281) and by the Singapore Ministry of Education Academic Research Fund Tier I (WBS No. R-144-000-353-112).

W. M., L. Z., and Q. Z. contributed equally to this work.

*Present address: School of Electronic Science and Applied Physics, Hefei University of Technology, Hefei 230009, China.
†fzshi@ustc.edu.cn
‡phygj@nus.edu.sg
§djf@ustc.edu.cn

[1] D. J. Thouless, Quantization of particle transport, Phys. Rev. B **27**, 6083 (1983).
[2] D. J. Thouless, M. Kohmoto, M. P. Nightingale, and M. den Nijs, Quantized Hall Conductance in a Two-Dimensional Periodic Potential, Phys. Rev. Lett. **49**, 405 (1982).
[3] M. Kohmoto, Topological invariant and the quantization of the Hall conductance, Ann. Phys. (N.Y.) **160**, 343 (1985).
[4] D. Xiao, M.-C. Chang, and Q. Niu, Berry phase effects on electronic properties, Rev. Mod. Phys. **82**, 1959 (2010).
[5] V. Gritsev and A. Polkovnikov, Dynamical quantum Hall effect in the parameter space, Proc. Natl. Acad. Sci. U.S.A. **109**, 6457 (2012).
[6] M. Switkes, C. M. Marcus, K. Campman, and A. C. Gossard, An adiabatic quantum electron pump, Science **283**, 1905 (1999).
[7] M. D. Blumenthal, B. Kaestner, L. Li, S. Giblin, T. J. B. M. Janssen, M. Pepper, D. Anderson, G. Jones, and D. A. Ritchie, Gigahertz quantized charge pumping, Nat. Phys. **3**, 343 (2007).
[8] B. Kaestner, V. Kashcheyevs, S. Amakawa, M. D. Blumenthal, L. Li, T. J. B. M. Janssen, G. Hein, K. Pierz, T. Weimann, U. Siegner, and H. W. Schumacher, Single-parameter nonadiabatic quantized charge pumping, Phys. Rev. B **77**, 153301 (2008).
[9] J. M. Shilton, V. I. Talyanskii, M. Pepper, D. A. Ritchie, J. E. F. Frost, C. J. B. Ford, C. G. Smith, and G. A. C. Jones, High-frequency single-electron transport in a quasi-one-dimensional GaAs channel induced by surface acoustic waves, J. Phys. Condens. Matter **8**, L531 (1996).
[10] S. Nakajima, T. Tomita, S. Taie, T. Ichinose, H. Ozawa, L. Wang, M. Troyer, and Y. Takahashi, Topological Thouless pumping of ultracold fermions, Nat. Phys. **12**, 296 (2016).
[11] M. Lohse, C. Schweizer, O. Zilberberg, M. Aidelsburger, and I. Bloch, A Thouless quantum pump with ultracold bosonic atoms in an optical superlattice, Nat. Phys. **12**, 350 (2016).
[12] Q. Niu, Towards a Quantum Pump of Electric Charges, Phys. Rev. Lett. **64**, 1812 (1990).
[13] J. P. Pekola, O.-P. Saira, V. F. Maisi, A. Kemppinen, M. Möttönen, Y. A. Pashkin, and D. V. Averin, Single-electron current sources: Toward a refined definition of the ampere, Rev. Mod. Phys. **85**, 1421 (2013).
[14] E. Berg, M. Levin, and E. Altman, Quantized Pumping and Topology of the Phase Diagram for a System of Interacting Bosons, Phys. Rev. Lett. **106**, 110405 (2011).
[15] D. Meidan, T. Micklitz, and P. W. Brouwer, Topological classification of interaction-driven spin pumps, Phys. Rev. B **84**, 075325 (2011).
[16] D. Rossini, M. Gibertini, V. Giovannetti, and R. Fazio, Topological pumping in the one-dimensional Bose-Hubbard model, Phys. Rev. B **87**, 085131 (2013).
[17] F. Grusdt and M. Höning, Realization of fractional Chern insulators in the thin-torus limit with ultracold bosons, Phys. Rev. A **90**, 053623 (2014).
[18] J. Tangpanitanon, V. M. Bastidas, S. Al-Assam, P. Roushan, D. Jaksch, and D. G. Angelakis, Topological Pumping of Photons in Nonlinear Resonator Arrays, Phys. Rev. Lett. **117**, 213603 (2016).
[19] P. L. e S. Lopes, P. Ghaemi, S. Ryu, and T. L. Hughes, Competing adiabatic Thouless pumps in enlarged parameter spaces, Phys. Rev. B **94**, 235160 (2016).
[20] E. Schrödinger, Die gegenwärtige situation in der Quantenmechanik, Naturwissenschaften **23**, 807 (1935); **23**, 823 (1935); **23**, 844 (1935); J. D. Trimmer, The present situation in quantum mechanics: A translation of Schrödinger's "Cat Paradox" paper, Proc. Am. Philos. Soc. **124**, 323 (1980); *Quantum Theory and Measurement*, edited by J. A. Wheeler and W. H. Zurek (Princeton University Press, Princeton, New Jersey, 1983), p. 152.
[21] T. Baumgratz, M. Cramer, and M. B. Plenio, Quantifying Coherence, Phys. Rev. Lett. **113**, 140401 (2014).
[22] P. Brumer and M. Shapiro, Control of unimolecular reactions using coherent light, Chem. Phys. Lett. **126**, 541 (1986).
[23] D. J. Tannor, R. Kosloff, and S. A. Rice, Coherent pulse sequence induced control of selectivity of reactions: Exact quantum mechanical calculations, J. Chem. Phys. **85**, 5805 (1986).
[24] L. Zhu, V. Kleiman, X. Li, S. P. Lu, K. Trentelman, and R. J. Gordon, Coherent laser control of the product distribution obtained in the photoexcitation of HI, Science **270**, 77 (1995).

[25] R. J. Glauber, Coherent, and incoherent states of the radiation field, Phys. Rev. **131**, 2766 (1963).
[26] M. O. Scully, Enhancement of the Index of Refraction via Quantum Coherence, Phys. Rev. Lett. **67**, 1855 (1991).
[27] A. Albrecht, Some remarks on quantum coherence, J. Mod. Opt. **41**, 2467 (1994).
[28] D. F. Walls and G. J. Milburn, *Quantum Optics* (Springer-Verlag, Berlin, 1995).
[29] M. O. Scully and M. S. Zubairy, *Quantum Optics* (Cambridge University Press, Cambridge, England, 1997).
[30] M. A. Nielsen and I. L. Chuang, *Quantum Computation and Quantum Information* (Cambridge University Press, Cambridge, England, 2000).
[31] S. L. Braunstein and C. M. Caves, Statistical Distance and the Geometry of Quantum States, Phys. Rev. Lett. **72**, 3439 (1994).
[32] V. Giovannetti, S. Lloyd, and L. Maccone, Quantum Metrology, Phys. Rev. Lett. **96**, 010401 (2006).
[33] V. Giovannetti, S. Lloyd, and L. Maccone, Advances in quantum metrology, Nat. Photonics **5**, 222 (2011).
[34] *Quantum Coherence in Solid State Systems*, Proceedings of the International School of Physics "Enrico Fermi", Vol. 171, edited by B. Deveaud-Pldran, A. Quattropani, and P. Schwendimann (IOS Press, Amsterdam, 2009), ISBN: 978-1-60750-039-1.
[35] C.-M. Li, N. Lambert, Y.-N. Chen, G.-Y. Chen, and F. Nori, Witnessing quantum coherence: From solid-state to biological systems, Sci. Rep. **2**, 885 (2012).
[36] L. H. Ford, Quantum coherence effects and the second law of thermodynamics, Proc. R. Soc. A **364**, 227 (1978).
[37] L. A. Correa, J. P. Palao, D. Alonso, and G. Adesso, Quantum-enhanced absorption refrigerators, Sci. Rep. **4**, 3949 (2014).
[38] V. Narasimhachar and G. Gour, Low-temperature thermodynamics with quantum coherence, Nat. Commun. **6**, 7689 (2015).
[39] M. Lostaglio, D. Jennings, and T. Rudolph, Description of quantum coherence in thermodynamic processes requires constraints beyond free energy, Nat. Commun. **6**, 6383 (2015).
[40] J. Åberg, Catalytic Coherence, Phys. Rev. Lett. **113**, 150402 (2014).
[41] N. Zhao, J.-L. Hu, S.-W. Ho, J. T. K. Wan, and R.-B. Liu, Atomic-scale magnetometry of distant nuclear spin clusters via nitrogen-vacancy spin in diamond, Nat. Nanotechnol. **6**, 242 (2011).
[42] N. Zhao, J. Honert, B. Schmid, M. Klas, J. Isoya, M. Markham, D. Twitchen, F. Jelezko, R.-B. Liu, H. Fedder, and J.Wrachtrup, Sensing single remote nuclear spins, Nat. Nanotechnol. **7**, 657 (2012).
[43] N. Zhao, S.-W. Ho, and R.-B. Liu, Decoherence and dynamical decoupling control of nitrogen vacancy center electron spins in nuclear spin baths, Phys. Rev. B **85**, 115303 (2012).
[44] G. S. Engel, T. R. Calhoun, E. L. Read, T.-K. Ahn, T. Mančal, Y.-C. Cheng, R. E. Blakenship, and G. R. Fleming, Evidence for wavelike energy transfer through quantum coherence in photosynthetic systems, Nature (London) **446**, 782 (2007).
[45] E. Collini, C. Y. Wong, K. E. Wilk, P. M. G. Curmi, P. Brumer, and G. D. Scholes, Coherently wired light-harvesting in photosynthetic marine algae at ambient temperature, Nature (London) **463**, 644 (2010).
[46] N. Lambert, Y.-N. Chen, Y.-C. Cheng, C.-M. Li, G.-Y. Chen, and F. Nori, Quantum Biology, Nat. Phys. **9**, 10 (2013).
[47] H. Wang, L. Zhou, and J. Gong, Interband coherence induced correction to adiabatic pumping in periodically driven systems, Phys. Rev. B **91**, 085420 (2015).
[48] L. Zhou, D. Y. Tan, and J. Gong, Effects of dephasing on quantum adiabatic pumping with nonequilibrium initial states, Phys. Rev. B **92**, 245409 (2015).
[49] A. Messiah, *Quantum Mechanics* (North-Holland, Amsterdam, 1962), Vol. II, p. 752.
[50] G. Rigolin, G. Ortiz, and V. H. Ponce, Beyond the quantum adiabatic approximation: Adiabatic perturbation theory, Phys. Rev. A **78**, 052508 (2008).
[51] See Supplemental Material at http://link.aps.org/supplemental/10.1103/PhysRevLett.120.120501 for theoretical and experimental details.
[52] In M. D. Schroer, M. H. Kolodrubetz, W. F. Kindel, M. Sandberg, J. Gao, M. R. Vissers, D. P. Pappas, A. Polkovnikov, and K. W. Lehnert, Measuring a Topological Transition in an Artificial Spin-1/2 System, Phys. Rev. Lett. **113**, 050402 (2014), this model was realized using a superconducting qubit. There, the system parameters (k, ϕ) were mapped differently onto the spherical angular coordinates of the spin Bloch sphere, and the band touching points $\delta_1/\delta_2 = \pm 1$ can be seen as topological phase transition points because the first Chern number defined on a spherical manifold makes a jump there. The Chern number was measured by use of a generalized force $\partial_\phi H(k, \phi)$ in response to the time variation of k.
[53] M. W. Doherty, N. B. Manson, P. Delaney, F. Jelezko, J. Wrachtrup, and L. C. L. Hollenberg, The nitrogen-vacancy colour centre in diamond, Phys. Rep. **528**, 1 (2013).
[54] R. Schirhagl, K. Chang, M. Loretz, and C. L. Degen, Nitrogen-vacancy centers in diamond: Nanoscale sensors for physics and biology, Annu. Rev. Phys. Chem. **65**, 83 (2014).
[55] S. Prawer and I. Aharonovich, *Quantum Information Processing with Diamond* (Woodhead Publishing, Cambridge, England, 2014).
[56] J. Wrachtrup and A. Finkler, Single spin magnetic resonance, J. Magn. Reson. **269**, 225 (2016).
[57] V. Jacques, P. Neumann, J. Beck, M. Markham, D. Twitchen, J. Meijer, F. Kaiser, G. Balasubramanian, F. Jelezko, and J. Wrachtrup, Dynamic Polarization of Single Nuclear Spins by Optical Pumping of Nitrogen-Vacancy Color Centers in Diamond at Room Temperature, Phys. Rev. Lett. **102**, 057403 (2009).
[58] T. van der Sar, Z. H. Wang, M. S. Blok, H. Bernien, T. H. Taminiau, D. M. Toyli, D. A. Lidar, D. D. Awschalom, R. Hanson, and V. V. Dobrovitski, Decoherence-protected quantum gates for a hybrid solid-state spin register, Nature (London) **484**, 82 (2012).
[59] The Hamiltonian of the electronic ground state of the NV center with a static magnetic field B applied along the NV axis (also the z axis) is $H_{\mathrm{NV}} = DS_z^2 + \gamma B S_z$, where S_z is the angular momentum operator for spin-1, $D = 2\pi \times 2870$ MHz is the zero-field splitting, and

$\gamma = 2\pi \times 2.8$ MHz/G is the gyromagnetic ratio of the NV electron.

[60] L. Robledo, L. Childress, H. Bernien, B. Hensen, P. F. A. Alkemade, and R. Hanson, High-fidelity projective read-out of a solid-state spin quantum register, Nature (London) **477**, 574 (2011).

[61] X. Rong, J. Geng, F. Shi, Y. Liu, K. Xu, W. Ma, F. Kong, Z. Jiang, Y. Wu, and J. Du, Experimental fault-tolerant universal quantum gates with solid-state spins under ambient conditions, Nat. Commun. **6**, 8748 (2015).

[62] B. L. Altshuler and L. I. Glazman, Pumping electrons, Science **283**, 1864 (1999).

[63] C. Rorres, The turn of the screw: Optimal design of an Archimedes screw, J. Hydraul. Eng. **126**, 72 (2000).

[64] G. Müller and J. Senior, Simplified theory of Archimedean screws, J. Hydraul. Eng. **47**, 666 (2009).